



Fabrication, Calibration, and Deployment of a Custom-Built Radiometer

Callum E. Flowerday¹, Ryan Thalman², Jaron C. Hansen¹

¹Department of Chemistry and Biochemistry, Brigham Young University, Provo, UT 84602, USA

²Department of Chemistry, Snow College, Richfield, UT 84701, USA

Correspondence to: Jaron C. Hansen (jhansen@chem.byu.edu)

Abstract. A custom-built spectroradiometric system was developed to measure spectral actinic flux for atmospheric photochemistry. The radiometer incorporates a UV-enhanced fibre optic cable, a compact CCD spectrograph, and an interchangeable polytetrafluoroethylene (PTFE) receiver head. Five receiver designs (domes, cones, and flat tops) were fabricated and evaluated for angular response and wavelength-dependent efficiency using collimated UV and visible LEDs. The variable cone design showed the most uniform angular sensitivity, minimizing the need for post-processing corrections. Wavelength calibration was conducted using emission LEDs from 265 to 523 nm, and the full system response was characterized from 196 to 888 nm. The system was evaluated in a controlled atmospheric chamber and in outdoor field conditions. Under clear skies, outdoor testing validated the radiometer's effectiveness in measuring photon fluxes with an 11.2% uncertainty. These photon fluxes were used to calculate photolysis rate constants (J-values) with an uncertainty of 15.3% for both NO₂ and O₃. Although not fully cosine-corrected, the radiometer demonstrated sufficient stability and repeatability for deployment in research settings, particularly where commercial instruments are unavailable. This study establishes a low-cost, customizable tool for actinic flux measurements in support of atmospheric photochemistry.

1 Introduction

Solar ultraviolet and visible (UV/Vis) radiation drives key atmospheric photochemical processes by initiating the photodissociation of molecules such as ozone, nitrogen dioxide, and formaldehyde (Finlayson-Pitts and Pitts, 2000; Seinfeld and Pandis, 1998). These reactions produce reactive radicals (e.g., OH, O(¹D)) that influence oxidative capacity, trace gas lifetimes, and the formation of secondary pollutants (Bohn et al., 2016). The rates of these reactions are quantified by photolysis rate constants (J-values), which are determined by the product of wavelength dependent molecular absorption cross sections (σ), quantum yields (Φ), and the actinic flux, *F*(Bohn et al., 2016; Bohn and Lohse, 2023).

Actinic flux refers to the omnidirectional photon flux per unit wavelength, integrating incoming radiation over a 4π steradian solid angle. Unlike planar irradiance, it represents the full radiative environment experienced by atmospheric molecules. Accurate actinic flux measurements are essential for calculating J-values, supporting chemical transport models, and evaluating



30

40

45



air quality and climate impacts (Bohn et al., 2016; Madronich, 1987). This flux is influenced by solar zenith angle, aerosol loading, surface reflectivity, cloud cover, and gaseous absorption (Finlayson-Pitts and Pitts, 2000; Seinfeld and Pandis, 1998). To achieve reliable actinic flux measurements, radiometers must have an isotropic angular response across all zenith and azimuth angles. However, practical limitations in receiver geometry, optical materials, and housing design introduce angular biases that require careful characterization and correction (Bohn et al., 2016; Jäkel et al., 2007). While full angular corrections using radiative transfer models have been developed for 2π receivers (Jäkel et al., 2007), simplified goniometric calibration remains a practical option for field deployment. Bohn et al.(Jäkel et al., 2007) demonstrated that cosine errors and receiver geometry can significantly affect actinic flux measurements, particularly in the near-UV below 350 nm. As a result, goniometric characterization is now a standard approach.

Instrumentation for actinic flux measurements has advanced from double-monochromator systems with photomultiplier tubes (PMTs)(Antonenko and Savina, 1992) to modern compact CCD-(Kuusk et al., 2002) and photodiode-array-based spectroradiometers (Thomas and Zalewski, 1992; Carballar et al., 2024; Eppeldauer, 2000; Andor and Johnson, 1998; Houston and Livigni, 2001). CCD detectors, as described by Jäkel et al. (Jäkel et al., 2007), offer improved UV-B sensitivity (290–315 nm) and rapid acquisition (<300 ms), making them suitable for dynamic environments like aircraft campaigns and chamber studies. However, these instruments require meticulous calibration, including spectral response, stray light rejection, dark current correction, and cosine error assessment (Bohn and Lohse, 2023). In addition to this, many still use single band flux measurements.

Drift in spectral sensitivity can compromise the accuracy of filter radiometers, particularly for J(O¹D) from the photolysis of O₃ and NO₂ (Bohn et al., 2016). Radiometers are widely used in both ground-based and airborne applications. Ground-based measurements are crucial in areas such as Utah's Wasatch Front, where ozone sources remain poorly understood (Flowerday et al., 2023a; Flowerday et al., 2023b; Quality, 2021, 2023). Airborne platforms, including HALO and Zeppelin NT, facilitate vertical profiling but require corrections for aircraft motion and shading effects (Bohn and Lohse, 2023). In laboratory chambers, radiometers quantify artificial UV fluxes for controlled photochemistry experiments.

Calibration is central to accurate measurements and involves wavelength alignment using emission sources, absolute sensitivity calibration with irradiance standards (e.g., NIST-traceable lamps), and angular response testing using goniometers (Habte et al., 2017; Huang et al., 2020; Kaisti et al., 2014). These steps minimize uncertainty in J-values for photolabile species like ozone and NO₂, which absorb strongly in the UV-B and UV-A (Bohn and Lohse, 2023; Jäkel et al., 2007). While the Leighton relationship provides a useful approximation for the photostationary balance between NO, NO₂, and O₃, direct measurements of J(NO₂) and J(O(¹D)) offer a more accurate and comprehensive view of local photochemistry, particularly under conditions where additional radical sources, deposition processes, or transport disrupt simple equilibrium assumptions. A custom-built spectroradiometric system was developed to measure spectral actinic flux for atmospheric photochemistry. The radiometer incorporates a UV-enhanced fibre optic cable, a compact CCD spectrograph, and an interchangeable receiver head. Five receiver designs (domes, cones, and flat tops) were fabricated from polytetrafluoroethylene (PTFE) and evaluated for angular response and wavelength-dependent efficiency using collimated UV and visible LEDs.





2 Methods

2.1 Experimental Setup

The radiometer consists of a PTFE head (McMaster-Carr, 8546K26) mounted on a black-painted aluminium plate to reduce reflections. A lens tube (ThorLabs, SM1M10) and UV-enhanced fibre optic cable (ThorLabs, BFL105HSO2) are threaded into the head and connected to a spectrograph (Ocean Optics, USB2000+). In configurations using a quartz rod (McMaster-Carr, 1357T141), the rod is inserted into the lens tube and secured with a 3D-printed bracket and retaining rings. The quartz rod was 6.35 mm diameter, 19 mm long and was inserted into the lens tube and slightly into the receiver to flatten the phase angle dependence of the receiver head.

Five receiver designs were evaluated: dome, cone, flat top, dome with variable wall thickness, and cone with variable wall thickness. These were evaluated based on their angular response to determine the design with the most isotropic performance.

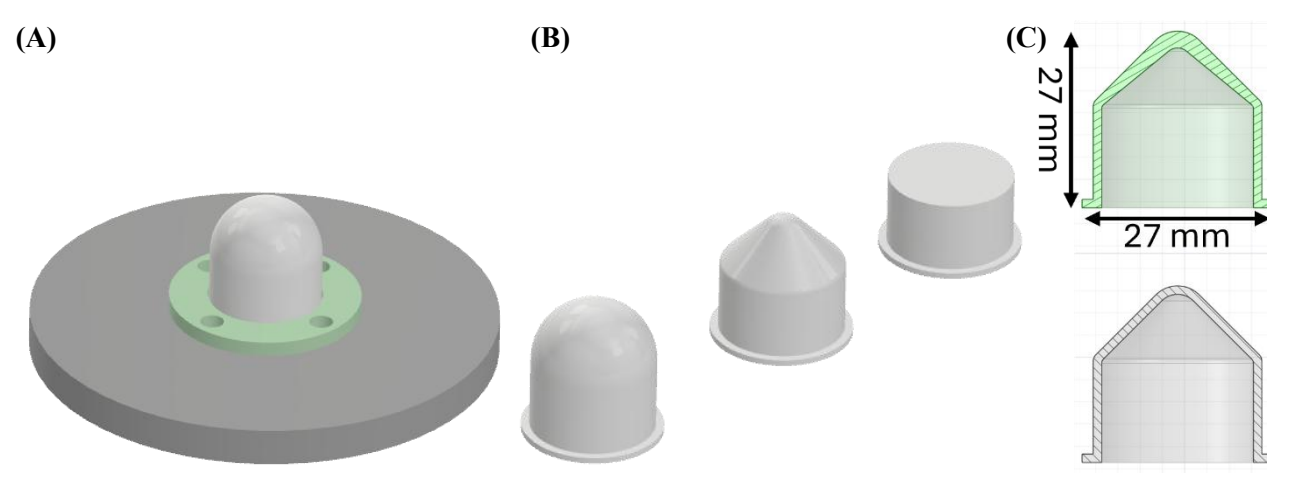


Fig. 1: (A) Radiometer receiver setup. (B) Radiometer head configurations shown as a dome, flat top, and cone (c) an illustration of what is meant by "varying wall thickness" in the cone receiver.

2.2 Wavelength Efficiency Calibration

Light-emitting diodes (LEDs) were used to calibrate the radiometer across different wavelengths and phase angles. The details for the LEDs used in calibration can be found in Table 1. Each LED was mounted on a copper heat sink with a Peltier cooler (DigiKey, CP30138) and a temperature controller (Meerstetter Engineering, TEC-1091) to minimize intensity drift.

Table 1. Details of LEDs used in the calibration of the radiometer

Wavelength (nm)	Provider	Part Number
265	DigiKey	3993-QLUXUVCR202W1LED-ND
310	Roithner Laser Technik	DUV310-SD353EN
325	Roithner Laser Technik	DUV325-SD353EV



90

95

100



340	Roithner Laser Technik	DUV340-SD353EL-01
375	Mouser Electronics	LZ1-10UVH0-0000
460	Mouser Electronics	897-LZ110B2020000
523	Mouser Electronics	720-LZ1-10G1020000G2

The receiver was mounted at the centre of a goniometer, and the light source was rotated from 0° to 180° in 10° increments to characterize angular sensitivity. The light source comprised a 50 mm f/1 lens (ThorLabs, LA4464) in front of a LED mounted on a copper heat sink with a Peltier cooler and a fan. This setup ensured the beam was collimated and filled the receiver head, while temperature control minimized LED output drift during calibration.

The calibration was repeated after rotating the receiver 90° to check for construction symmetry. LED power was measured before and after calibration to convert intensity readings into wavelength-dependent power. For these measurements, the LED light was focused onto the power meter using the same lens, ensuring the beam filled the meter's aperture. The radiometer output spanned 196–888 nm with 0.38 nm spacing and 2.5 nm FWHM resolution.

2.3 Chamber and field deployment

The radiometer was evaluated in an atmospheric chamber and outside with a solar flux. The atmospheric chamber is made of 0.127 mm thick fluorinated ethylene propylene (FEP) film (AirTech) to make a chamber that has a volume of approximately 35 m³. All inlets and outlets to the bag pass through a 6.35 mm thick PTFE plate (0.91 × 1.22 m) that serves as the base to the atmospheric chamber (Interstate Advanced Materials). The bag was sealed to the plate using polyester masking tape with a silicon adhesive (Advanced Polymer Tape). Above the chamber is a bank of fifty-six 36 W UVC (1000Bulbs.com, G36T8) and fourteen 75 W UVC (Canadalite.com, TUV75WHO) bulbs. The outside testing took place on the campus of Brigham Young University, Provo, Utah, USA (40.2518° N, 111.6493° W) on 10 July 2025 from 9:19-15:49 MDT. Clear, warm summer conditions prevailed, with temperatures ranging from approximately 26–32 °C. (Time and Date, 2025; Timeanddate.Com, 2025) Low mid-afternoon humidity (23–37 %) and light breeze (<5 m/s) created stable atmospheric conditions ideal for accurate radiometric measurements. Spectra were collected every 3 ms, and 20,000 spectra were averaged during acquisition to produce one spectrum per minute during field testing. These were scaled to a 1-second integration time and used to calculate irradiance (W/m²/s) and photon flux (photons/cm²/s).

2.4 TUV Model Configuration

105 The NCAR Tropospheric Ultraviolet and Visible (TUV v5.3) model (Madronich and Flocke, 1999) was used to simulate actinic flux and photolysis rates for the field experiment. Model inputs matched the measurement conditions: latitude 40.23°, longitude –111.67°, date 2025-07-10, and altitude 1.4 km a.s.l. The surface albedo was 0.9999, overhead ozone column 310 DU, and temperature 298 K. Clouds and aerosols were omitted (optical depth = 0), and the pseudo-spherical four-stream solver



115

120

125



was used for higher accuracy. Outputs included actinic flux (quanta s⁻¹ cm⁻² nm⁻¹), cross-sections, and quantum yields. These parameters are provided here for transparency and to facilitate replication.

3 Results and discussion

3.1 Radiometer configurations

Among the tested receivers, the one showing the least sensitivity to phase angle is the optimal choice, as it minimizes, or even removes, the need for post-acquisition correction, thereby reducing uncertainty in the final results. As such, five receiver shapes and configurations were evaluated and compared for the best use outside in a field setting and in a chamber setting. Fig. 2 shows a representation of the measured phase angle dependences in the UV. These shapes and trends were consistent across the six calibration wavelengths.

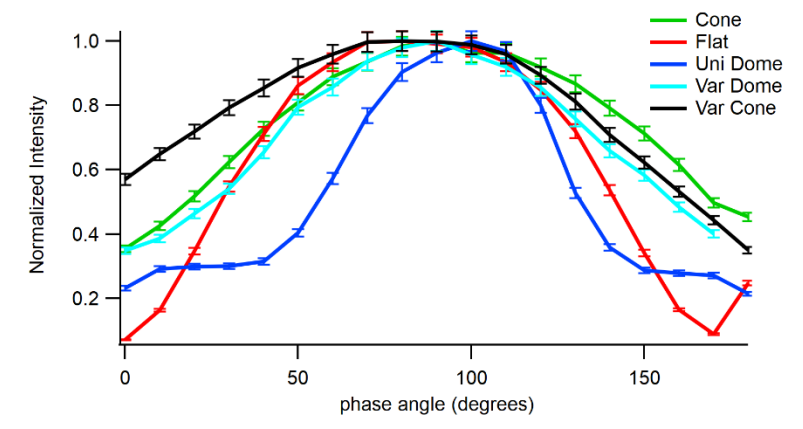


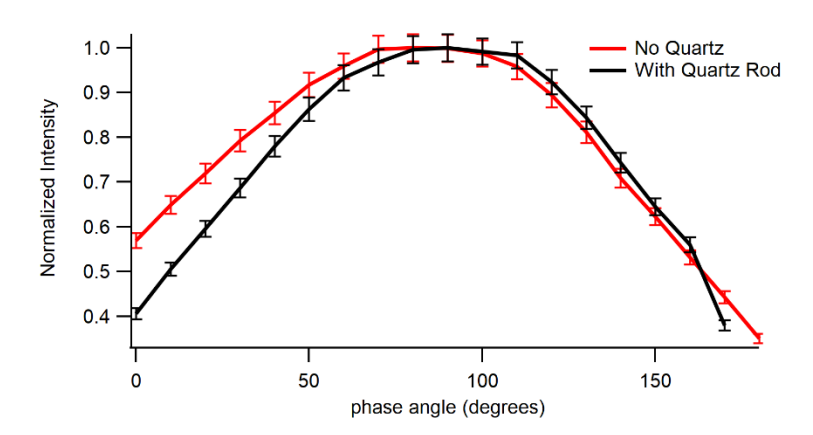
Fig. 2: Comparison of phase angle dependence for each receiver at 310 nm: dome (blue), cone (green), flat (red), dome with varying wall thickness (cyan), cone with varying wall thickness (black).

Angular-response testing included both zenith and azimuthal assessments. Receiver rotation by 90° confirmed < 10 % asymmetry between orthogonal orientations, indicating that the variable-cone design closely approximates a cosine response. Although a full two-dimensional angular correction was not applied, the observed isotropy suggests that solar-angle biases are small under the clear-sky conditions tested. Future work will incorporate radiative-transfer-based 2-D correction following Jäkel et al. (Jäkel et al., 2007) and Bohn & Lohse (Bohn and Lohse, 2023).

As shown in Fig. 3, while the light throughput of the radiometer increased, the quartz rod did not assist in flattening out the phase angle dependence of the receiver. The radiometer is not light limited; therefore, it was simpler to not use a quartz rod moving forward as the increased light throughput was not needed in this instrument.

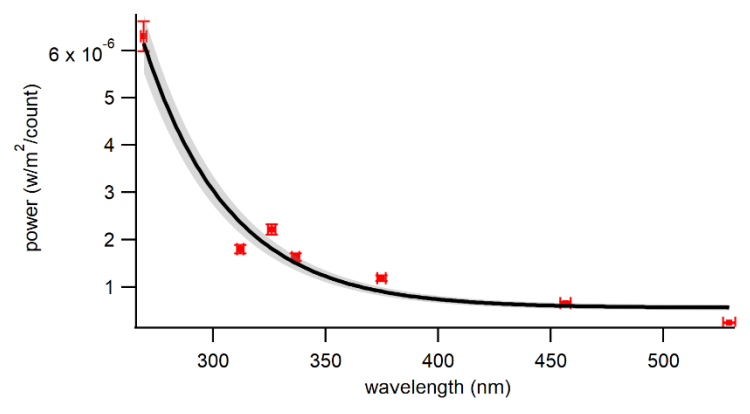






130 Fig. 3: Comparison of phase angle dependence of the flat top receiver with (black) and without (red) the quartz rod at 310 nm.

The wavelength efficiency of the radiometer was slightly different depending on which receiver head was used; however, the wavelength efficiency of the radiometer followed the same trends as the quantum efficiency of the spectrograph. Fig. 4 shows an example of a wavelength efficiency curve that was used in calculating flux with the radiometer.



135 Fig. 4: The wavelength efficiency curve for the variable cone receiver configuration of the radiometer. Grey shading indicates the 10% error in the fit line.

Stray-light performance was verified prior to calibration by illuminating the spectrograph with isolated mercury emission lines. No secondary broad features were observed, indicating minimal leakage into adjacent wavelength regions. The original grating was replaced with a broadband UV-visible grating (200-888 nm) to reduce out-of-band scatter, eliminating the minor stray-light signal initially observed. Residual stray-light contributions are therefore estimated to be negligible.

3.2 Error Propagation

140

The error in the calibration of the radiometer was a combination of the error in the wavelength stamp of the spectrograph (0.5%), the error in the power meter (5%), and the error in the fit function used to create the calibration curve (10%). These were combined in quadrature for a total error in calibration of 11.2%. This was also the error in the flux measurements.





The error in the calculation of the J-values in the formation of O^1D from the photolysis of NO_2 and O_3 includes the uncertainty in the absorption cross-sections of NO_2 , 3% (Vandaele et al., 1998), and O_3 , 3.1% (Bogumil et al., 2003), and the uncertainty in the quantum yields of NO_2 , 10% (Troe, 2000), and O_3 , 10% (Matsumi et al., 2002). Total errors were calculated in quadrature for the flux measurements of J_{NO_2} and J_{O_3} as 15.3% and 15.3%, respectively.

3.3 Chamber Deployment

The radiometer receiver was placed on the chamber floor at its centre, where light intensity was highest. A fibre optic cable connected the receiver through the floor to a spectrograph positioned below the chamber. The chamber's light bank emitted light primarily between 50° and 130°, with 90° directly above the receiver. In this range, the flat-top radiometer showed minimal dependence on phase angle and was therefore selected for these experiments. The total output of the lamp array above the chamber was measured at 21.8 W.

155 Fig. 5 shows the measured photon flux in the chamber. The expected mercury emission lines and the broad peak around 360 nm from the UVC and UVB lamps were clearly captured. Although the chamber's photon flux is lower than solar noon on a clear, average summer day, it remains sufficiently strong for photochemical studies. The integrated photon flux from 250-600 nm in the chamber is 3.13×10^{14} photons/cm²/s.

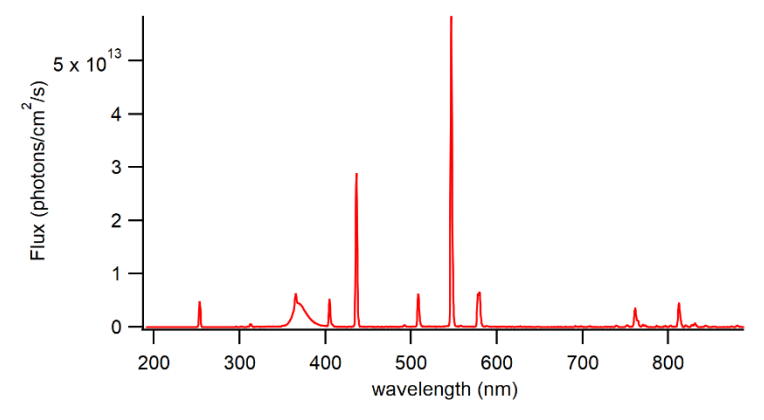


Fig. 5: Spectrum of the measured photon flux in chamber experiment. This spectrum is a combination of UVC and UVB lamps.

3.4 Field Deployment

160

165

Measured photon fluxes from field deployment can be seen in Fig. 6(A). An intensity vs time trace is shown in Fig. 6(B) to show part of the diurnal pattern measured during this experiment. It should be noted that spectra are reported in photon-flux units (photons cm⁻² s⁻¹ nm⁻¹) rather than energy-flux units (W m⁻² nm⁻¹), the solar maximum appears near 550 nm rather than \approx 500 nm. This shift is consistent with the ASTM G-173 AM 1.5 G reference spectrum when expressed in photon units and reflects the wavelength dependence of the photon-energy conversion. The total flux measured from 300-888 nm, the wavelength range of light seen in the spectrometer, is $6.19 \pm 0.69 \times 10^{17}$ photons/cm²/s. The flux at each wavelength was on the order of 10^{14} photons/cm²/s. These values are consistent with other work done at similar conditions (Finlayson-Pitts and



170

175

180

185

190

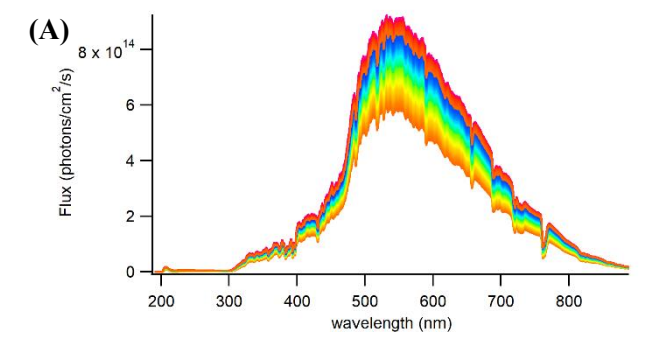


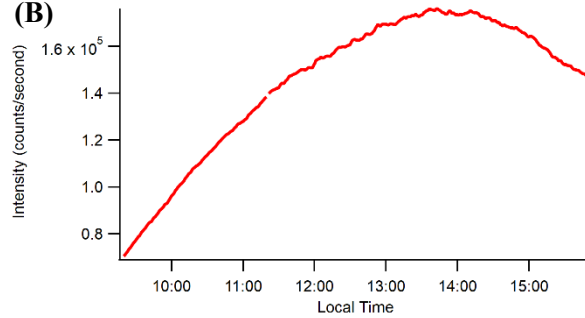
Pitts, 2000; Madronich et al., 1983; Hofzumahaus et al., 1999; Monks et al., 2004; Kim et al., 2007; Li et al., 2020; Peterson, 1976). Integrated J-values were then calculated using Equation 1:

$$J_{\lambda} = \int \Phi(\lambda)\sigma(\lambda)I(\lambda)d(\lambda) , \qquad (1)$$

where $\Phi(\lambda)$ is the wavelength specific quantum yield, $\sigma(\lambda)$ the wavelength specific absorption cross-section, and $I(\lambda)$ the wavelength specific measured irradiance. Quantum yield values for the formation of O¹D from NO₂ (Troe, 2000) and O₃ (Matsumi et al., 2002) photolysis were taken from the JPL Evaluation (Jet Propulsion, 2019). These were interpolated to match the spectrometer's wavelength stamp. Absorption cross-sections were obtained from Vandaele et al. (Vandaele et al., 1998) for NO₂ and Bogumil et al. (Bogumil et al., 2003) for O₃. J-values for NO₂ were found to peak on the order of 10⁻² s⁻¹ and on the order of 10⁻⁵ for O₃. These values are consistent with other work done at similar conditions (Stockwell and Goliff, 2004; Cotte et al., 1997; Reuder et al., 1996; Beine et al., 1999; Hofzumahaus et al., 2004; Trebs et al., 2009). Measured J-values were also compared to the NCAR Tropospheric Ultraviolet and Visible (TUV) Radiation Model (Madronich and Flocke, 1999) and AtChem (Sommariva et al., 2020) using the conditions described earlier in the paper. The measured are in close agreement with the modelled values being less than a factor of 3 different. The measured J-values showed close agreement with the TUV radiative transfer model results (Fig. 6 C-D). For both NO₂ and O₃, the model reproduced the diurnal behaviour and magnitude of photolysis frequencies with deviations generally within the propagated measurement uncertainty (±15.3 %). Morning J(NO₂) values were slightly overestimated by the model relative to measurements, which may reflect unaccounted cloud or aerosol scattering. Such effects can attenuate short-wavelength actinic flux and are not represented in the clear-sky TUV configuration used here. Minor discrepancies and uncertainties in defined quantum yield and absorption cross-sections can also account for this deviation.

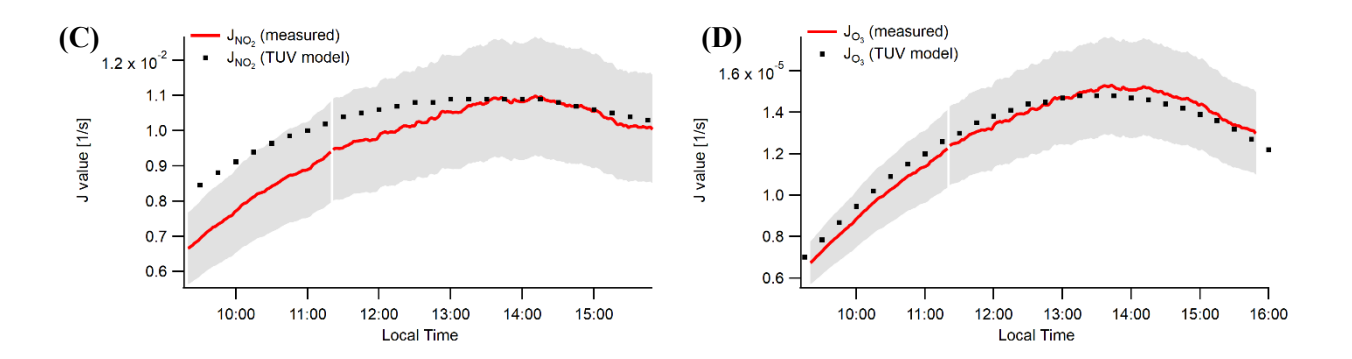
The J(O₃) photolysis rate, by contrast, was well captured across the full period after accounting for the temperature- and pressure-dependent quantum yield of O(¹D) formation (Matsumi et al., 2002). Correcting the literature quantum yields to local conditions improved agreement between measured values and modelled values. Overall, the strong correlation between modelled and measured J-values validates both the wavelength calibration and the absolute response of the radiometer.











195 Fig. 6: (A) Measured flux, in photons/cm²/s, for the duration of the experiment. Each individual spectrum is coloured differently. (B) Time trace of intensity at a single wavelength, 311 nm, for the duration of the experiment (C) Comparison of measured J(NO₂) values (red) with TUV model outputs (black squares); shaded area denotes propagated uncertainty (±15.3 %).. (D) Comparison of measured J(O₃) values (red) with TUV model outputs (black squares); shaded area denotes propagated uncertainty (±15.3 %). Both modeled and measured datasets show strong agreement, with minor overestimation of J(NO₂) during early morning hours likely due to transient aerosol or cloud scattering effects not included in the model.

4. Conclusions

205

210

This study details the development and evaluation of a compact, cost-effective radiometer for measuring actinic flux in the UV/Vis spectral range. A custom-built spectroradiometric system was constructed, incorporating a UV-enhanced fibre optic cable, a CCD spectrograph, and an interchangeable PTFE receiver head. Five receiver designs—domes, cones, and flat tops—were fabricated and evaluated for angular response and wavelength-dependent efficiency using collimated UV and visible LEDs.

Through iterative testing and calibration across multiple wavelengths, the variable cone receiver was identified as the optimal configuration due to its minimized phase angle dependence. While the use of a quartz rod increased light throughput, it did not improve angular response uniformity and was thus excluded in field deployments. The radiometer exhibited reliable performance during both chamber and ambient solar tests, demonstrating suitability for photolysis rate calculations.

Although angular response was characterized, post-processing cosine corrections were not applied. Stray light effects, while not explicitly corrected, were expected to be minimal due to the spectrometer's wavelength range and low saturation levels. Future enhancements could include improved stray light rejection and more precise goniometric calibration. Stability over time is particularly important for broadband instruments used in long-term or field deployments.

215 Comparison with the TUV model under clear-sky assumptions confirmed the instrument's calibration accuracy, with temperature- and pressure-corrected J(O₃) rates agreeing closely and early-morning J(NO₂) differences likely arising from transient aerosol or cloud attenuation.

With proper calibration, the radiometer provides a robust platform for atmospheric photochemistry studies in both laboratory and field environments. Accurate spectral actinic flux measurements are foundational for calculating photolysis rates in



225



atmospheric chemistry. Continued development and calibration of radiometers capable of resolving UV/Vis flux remain critical to advancing our understanding of atmospheric oxidation, air quality, and climate-relevant photochemistry.

Author Contributions: C.E.F: Conceptualization, writing of the original manuscript, data acquisition, data analysis. **R.T.:** Original project design, conceptualization, data analysis, writing review and editing, funding acquisition. **J.C.H.:** writing review and editing, supervision, and funding acquisition. All Authors have read and agreed to the published version of the manuscript.

Data Availability Statement: Available on BYU's Scholar's archive (https://scholarsarchive.byu.edu/data/87)

Declaration of conflicts: the author(s) declare no conflicts of interest.

Funding: Student salaries and supplies were provided by the College of Physical and Mathematical Sciences at Brigham Young University. This work was supported by the National Science Foundation, grant #2321381. The funder played no role in the study design, data collection, analysis and interpretation of data, or the writing of this manuscript.

References

- Andor, G. and Johnson, B. C.: Short-term stability measurements of a germanium photodiode radiometer, Metrologia, 35, 517-521, 10.1088/0026-1394/35/4/53, 1998.
- Antonenko, G. I. and Savina, V. I.: Radiometer for Testing the Natural C-14 Level, Instruments and Experimental Techniques, 35, 696-698, 1992.
 - Beine, H. J., Dahlback, A., and Ørbæk, J. B.: Measurements of J(NO2) at Ny-Ålesund, Svalbard, Journal of Geophysical Research: Atmospheres, 104, 16009-16019, https://doi.org/10.1029/1999JD900237, 1999.
 - Bogumil, K., Orphal, J., Homann, T., Voigt, S., Spietz, P., Fleischmann, O. C., Vogel, A., Hartmann, M., Kromminga, H.,
- Bovensmann, H., Frerick, J., and Burrows, J. P.: Measurements of molecular absorption spectra with the SCIAMACHY preflight model: instrument characterization and reference data for atmospheric remote-sensing in the 230-2380 nm region, Journal of Photochemistry and Photobiology a-Chemistry, 157, 167-184, 10.1016/s1010-6030(03)00062-5, 2003.
 - Bohn, B. and Lohse, I.: Optical receiver characterizations and corrections for ground-based and airborne measurements of spectral actinic flux densities, Atmospheric Measurement Techniques, 16, 209-233, 10.5194/amt-16-209-2023, 2023.
- Bohn, B., Heard, D. E., Mihalopoulos, N., Plass-Dülmer, C., Schmitt, R., and Whalley, L. K.: Characterisation and improvement of j(O1D) filter radiometers, Atmos. Meas. Tech., 9, 3455-3466, 10.5194/amt-9-3455-2016, 2016. Carballar, A., Rodríguez-Garrido, R., Jerez, M., Vera, J., and Granado, J.: Measuring DNI with a New Radiometer Based on an Optical Fiber and Photodiode, Sensors, 24, 3674, 2024.
- Cotte, H., Devaux, C., and Carlier, P.: Transformation of Irradiance Measurements into Spectral Actinic Flux for Photolysis Rates Determination, Journal of Atmospheric Chemistry, 26, 1-28, 10.1023/A:1005763127365, 1997.
 - Eppeldauer, G. P.: Noise-optimized silicon radiometers, Journal of Research of the National Institute of Standards and Technology, 105, 209-219, 10.6028/jres.105.027, 2000.
 - Finlayson-Pitts, B. J. and Pitts, J. N.: Chemistry of the Upper and Lower Atmosphere, Academic Press, San Diego, California2000.
- Flowerday, C. E., Thalman, R., and Hansen, J. C.: Twenty-Year Review of Outdoor Air Quality in Utah, USA, Atmosphere, 14, 1496, 2023a.
 - Flowerday, C. E., Thalman, R., and Hansen, J. C.: Local and Regional Contributions to Tropospheric Ozone Concentrations, Atmosphere, 14, 10.3390/atmos14081262, 2023b.
- Habte, A., Sengupta, M., Andreas, A., Reda, I., and Robinson, J.: Radiometer calibration methods and resulting irradiance differences, Progress in Photovoltaics, 25, 614-622, 10.1002/pip.2812, 2017.





- Hofzumahaus, A., Kraus, A., and Müller, M.: Solar actinic flux spectroradiometry: a technique for measuring photolysis frequencies in the atmosphere, Applied Optics, 38, 4443-4460, 10.1364/AO.38.004443, 1999.
- Hofzumahaus, A., Lefer, B. L., Monks, P. S., Hall, S. R., Kylling, A., Mayer, B., Shetter, R. E., Junkermann, W., Bais, A., Calvert, J. G., Cantrell, C. A., Madronich, S., Edwards, G. D., Kraus, A., Müller, M., Bohn, B., Schmitt, R., Johnston, P.,
- 265 McKenzie, R., Frost, G. J., Griffioen, E., Krol, M., Martin, T., Pfister, G., Röth, E. P., Ruggaber, A., Swartz, W. H., Lloyd, S. A., and Van Weele, M.: Photolysis frequency of O3 to O(1D):: Measurements and modeling during the International Photolysis Frequency Measurement and Modeling Intercomparison (IPMMI) -: art. no. D08S90, Journal of Geophysical Research-Atmospheres, 109, 10.1029/2003jd004333, 2004.
- Houston, J. M. and Livigni, D. J.: Comparison of two cryogenic radiometers at NIST, Journal of Research of the National Institute of Standards and Technology, 106, 641-647, 10.6028/jres.106.029, 2001.
 - Huang, X., Li, X., Zheng, X., Wei, W., and Wang, Y.: Radiometric calibration of a field transfer radiometer, Optik, 206, 164294, https://doi.org/10.1016/j.ijleo.2020.164294, 2020.
 - Jäkel, E., Wendisch, M., Blumthaler, M., Schmitt, R., and Webb, A. R.: A CCD Spectroradiometer for Ultraviolet Actinic Radiation Measurements, Journal of Atmospheric and Oceanic Technology, 24, 449-462, https://doi.org/10.1175/JTECH1979.1, 2007.
- 275 https://doi.org/10.1175/JTECH1979.1, 2007.
 Jet Propulsion, L.: Chemical Kinetics and Photochemical Data for Use in Atmospheric Studies, Evaluation No. 19, JPL Publication 19-5, Pasadena, California, USA, 2019.
 - Kaisti, M., Altti, M., and Poutanen, T.: Uncertainty of Radiometer Calibration Loads and Its Impact on Radiometric Measurements, Ieee Transactions on Microwave Theory and Techniques, 62, 2435-2446, 10.1109/tmtt.2014.2349873, 2014.
- 280 Kim, D., Loughner, C. P., Wetzel, M. A., Goliff, W. S., and Stockwell, W. R.: A comparison of photolysis rate parameters estimated from measured and simulated actinic flux for wintertime conditions at Storm Peak Laboratory, Colorado, Journal of Atmospheric Chemistry, 57, 59-71, 10.1007/s10874-007-9061-2, 2007.
 - Kuusk, A., Nilson, T., and Paas, M.: Angular distribution of radiation beneath forest canopies using a CCD-radiometer, Agricultural and Forest Meteorology, 110, 259-273, https://doi.org/10.1016/S0168-1923(02)00002-3, 2002.
- 285 Li, J. H. Y., Zhang, X., Orlando, J., Tyndall, G., and Michalski, G.: Quantifying the nitrogen isotope effects during photochemical equilibrium between NO and NO2: implications for δ15N in tropospheric reactive nitrogen, Atmospheric Chemistry and Physics, 20, 9805-9819, 10.5194/acp-20-9805-2020, 2020.
 - Madronich, S.: Photodissociation in the Atmosphere: Actinic Flux and the Effects of Ground Reflections and Clouds, Journal of Geophysical Research-Atmospheres, 92, 9740-9752, 10.1029/JD092iD08p09740, 1987.
- Madronich, S. and Flocke, S.: The Role of Solar Radiation in Atmospheric Chemistry, in: Environmental Photochemistry, The
 Handbook of Environmental Chemistry, Springer-Verlag, Berlin, Heidelberg, 1-26, 1999.
 Madronich, S., Hastie, D. R., Ridley, B. A., and Schiff, H. I.: Measurement of the Photodissociation Coefficient of NO2 in the
 - Atmosphere 1. Method and Surface Measurements, Journal of Atmospheric Chemistry, 1, 3-25, 10.1007/bf00113977, 1983. Matsumi, Y., Comes, F. J., Hancock, G., Hofzumahaus, A., Hynes, A. J., Kawasaki, M., and Ravishankara, A. R.: Quantum
- 295 yields for production of O(1D) in the ultraviolet photolysis of ozone: Recommendation based on evaluation of laboratory data, Journal of Geophysical Research: Atmospheres, 107, ACH 1-1-ACH 1-12, https://doi.org/10.1029/2001JD000510, 2002. Monks, P. S., Rickard, A. R., Hall, S. L., and Richards, N. A. D.: Attenuation of spectral actinic flux and photolysis frequencies at the surface through homogenous cloud fields, Journal of Geophysical Research-Atmospheres, 109, 10.1029/2003jd004076,
- Peterson, J. T.: Calculated Actinic Fluxes (290–700 nm) for Air Pollution Applications, EPA-600/4-76-025, U.S. Environmental Protection Agency, Research Triangle Park, North Carolina, USA, 1976. What is Ozone?: https://deq.utah.gov/air-quality/what-is-ozone, last access: 02/02/2023.
 - Ozone: EPA Designates Marginal Nonattainment Areas in Utah: https://deq.utah.gov/air-quality/ozone-marginal-nonattainment-areas-utah, last
- Reuder, J., Gori, T., Kins, L., and Dlugi, R.: Determination of photolysis frequencies of ozone and nitrogen dioxide during SANA 2: The influence of tropospheric aerosol particles, Meteorologische Zeitschrift, 5, 234-244, 10.1127/metz/5/1996/234, 1996.
 - Seinfeld, J. H. and Pandis, S. N.: Atmospheric Chemistry and Physics: From Air Pollution to Climate Change, Wiley-Interscience, New York, USA1998.





- Sommariva, R., Cox, S., Martin, C., Boronska, K., Young, J., Jimack, P. K., Pilling, M. J., Matthaios, V. N., Nelson, B. S., Newland, M. J., Panagi, M., Bloss, W. J., Monks, P. S., and Rickard, A. R.: AtChem (version 1), an open-source box model for the Master Chemical Mechanism, Geoscientific Model Development, 13, 169-183, 10.5194/gmd-13-169-2020, 2020.
 Stockwell, W. R. and Goliff, W. S.: Measurement of actinic flux and the calculation of photolysis rate parameters for the Central California Ozone Study, Atmospheric Environment, 38, 5169-5177, https://doi.org/10.1016/j.atmosenv.2004.05.048,
 2004.
- Thomas, D. B. and Zalewski, E. F.: A Radiometer for Precision Coherent Radiation Measurements, Journal of Research of the National Institute of Standards and Technology, 97, 327-334, 10.6028/jres.097.012, 1992.

 Trebs, I., Bohn, B., Ammann, C., Rummel, U., Blumthaler, M., Königstedt, R., Meixner, F. X., Fan, S., and Andreae, M. O.: Relationship between the NO2 photolysis frequency and the solar global irradiance, Atmospheric Measurement Techniques,
- 2, 725-739, 10.5194/amt-2-725-2009, 2009.
 Troe, J.: Are primary quantum yields of NO2 photolysis at λ <= 398 nm smaller than unity?, Zeitschrift für Physikalische Chemie, 214, 573-581, 10.1524/zpch.2000.214.5.573, 2000.
 Vandaele, A. C., Hermans, C., Simon, P. C., Carleer, M., Colin, R., Fally, S., Merienne, M. F., Jenouvrier, A., and Coquart, B.: Measurements of the NO₂ absorption cross-section from 42 000 cm<SUP>-1</sli>
 1
 1
 1
 1
 1
 1
 1
 1
 1
 1
 1
 1
 1
 1
 1
 1
 1
 1
 1
 1
 1
 1
 1
 1
 1
 1
 1
 1
 1
 1
 1
 1
 1
 1
 1
 1
 1
 1
 1
 1
 1
 1
 1
 1
 1
 1
 1
 1
 1
 1
 1
 1
 1
 1
 1
 1
 1
 1
 1
 1
 1
 1
 2
 2
 3
 2
 3
 2
 3
 4
 4
 5
 6
 7
 7
 8
 9
 9
 1
 1
 1
 2
 2
 3
 2
 3
 2
 3
 3
 4
 5
 5
 6
 7
 8
 9
 9
 9
 9
 9
 9
 9
 9
 9
 9
- 325 1</SUP> (238-1000 nm) at 220 K and 294 K, Journal of Quantitative Spectroscopy & Radiative Transfer, 59, 171-184, 10.1016/s0022-4073(97)00168-4, 1998.